ACS OMEGA

http://pubs.acs.org/journal/acsodf

Article

# Layered Molybdenum (Meta)phosphate for Photoreduction of Hexavalent Chromium and Degradation of Methylene Blue under Sunlight Radiance

Omkar V. Vani and Anil M. Palve*

Cite This: *ACS Omega* 2022, 7, 26632−26640

Read Online

ACCESS | Metrics & More | Article Recommendations | Supporting Information

**ABSTRACT:** Noble metal, semiconductor, or metal-free nanomaterials have shown promising applicability as potential photocatalyst materials. A one-step process has been established for the synthesis of layered molybdenum (meta)phosphate [$MoO_2(PO_3)_2$] using a solvothermal method. The nanopowders were characterized by X-ray diffraction (XRD), UV−visible spectroscopy (UV−vis), scanning electron microscopy (SEM), infrared spectroscopy (IR), X-ray photoelectron spectroscopy (XPS), photoluminescence spectroscopy (PL), surface area analysis (Brunauer−Emmett−Teller (BET)), electron spin resonance (ESR), and high-resolution transmission electron microscopy (HRTEM). Through this study, we demonstrate the use of $MoO_2(PO_3)_2$ as a photocatalyst for wastewater treatment. The photoreduction of toxic $Cr^{6+}$ to $Cr^{3+}$ by layered molybdenum (meta)phosphate is investigated using formic acid as a scavenger. This catalyst has also been used for photodegrading organic dyes like methylene blue. $MoO_2(PO_3)_2$ has been shown to complete photoreduction of toxic $Cr^{6+}$ to $Cr^{3+}$ in 6 min and achieved 78% degradation efficiency for methylene blue in 36 min. The reactive species trapping experiments revealed that the key active species like $O_2^{\bullet-}$, $^{\bullet}OH$, and $h^+$ can exist and play an important role in methylene blue photodegradation.

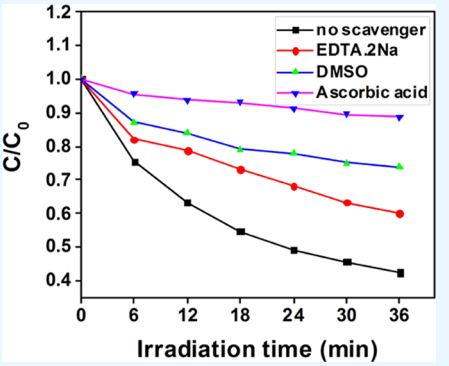


## 1. INTRODUCTION

For decades, population growth, urbanization, and industrialization have resulted in energy depletion and environmental pollution. Many effluents discharged by industries into water resources endanger aquatic life and the lives of downstream users. These effluents are classified as inorganic or organic pollutants. Hexavalent chromium is the most toxic heavy metal cation due to its cytotoxic, mutagenic, and carcinogenic properties.[1] Because of its ability to produce responsive oxygen species in cells, it is extremely toxic to all faunae.[2] Chromium exists in $Cr^{6+}$ to $Cr^{3+}$ oxidation states, with $Cr^{6+}$ being more toxic and causing more carcinogenic effects than trivalent chromium.[3] Chromium alloys are corrosion inhibitors and are useful in metal plating, leather tanning, and pigment manufacturing.[4] $Cr^{6+}$ is released in water and soil matters without any pretreatment from these industries, and it is nonbiodegradable and remains in the environment for a long time, causing a harmful effect.[5] It is possible to reduce it from hexavalent to trivalent using a suitable photocatalyst and then remove it using a precipitating agent such as sodium hydroxide.[6] Organic cationic methylene blue, methyl orange, and rhodamine-B were also released into the environment from the dye industries, affecting human health.[7] When methylene blue is released into water resources, it can cause eutrophication, perturbations, and harm to the water ecosystem.[8,9]

According to a literature survey, UV−visible light sources and natural sunlight are suitable for the removal of toxic pollutants.[10,11] For the remediation of these pollutants, different methods such as chemical oxidation, extraction, adsorption, photocatalytic, and biochemical processes were used.[12] Metals, a semiconducting material, and their composites are currently being investigated as photocatalysts for converting them into less-polluting materials. Pd nanoparticles are used for the catalytic reduction of $Cr^{6+}$ in the presence of formic acid.[13] Several semiconductor materials, including CdS/$CuInS_2$,[14] ZnO,[15] and $Cd_{0.5}Zn_{0.5}S$@ZIF-8,[16] have been reported for the photoreduction of $Cr^{6+}$. Recently, $MoSe_2$/ZnO/ZnSe[17] hybrid materials demonstrated complete $Cr^{6+}$ to $Cr^{3+}$ reduction. Carbon materials like carbon/palladium nanocomposites[18] and activated carbon-supported ZnO[19] nanocomposites have also been used to reduce $Cr^{6+}$. Sedimentation, chemical precipitation, adsorption, biological membranes, and ion-exchange processes have all been used to remove this harmful dye. These methods proved time-

Received: May 6, 2022
Accepted: July 13, 2022
Published: July 22, 2022

consuming and expensive, and the dye removal required a complicated process.[20] Semiconducting materials, such as Fe-ZnO,[21] $TiO_2$,[22] and ZnO/CdO,[23] were found to be useful for methylene blue degradation. Carbon materials as well as semiconductors such as $DyVO_4$/g-$C_3N_4I$[24] and C-doped $TiO_2$[25] have also been shown to degrade methylene blue. $TiO_2$ is the most extensively studied compound among those listed above due to its lack of toxicity, chemical stability, low cost, and superior catalytic properties.[26] The main impediment to $TiO_2$ commercialization is its band gap, absorption in only ultraviolet (UV) light, low recyclability of $TiO_2$ particles, and low adsorption capacity for hydrophobic pollutants.[27] To overcome the weaknesses of titanium oxide, numerous materials for photocatalytic applications have been tested.[28]

Molybdenum has several oxidation states, and its phosphate exists in different forms such as mono ($PO_4^{3-}$), di-or (pyro $P_2O_7^{4-}$), meta ($PO_3^{3-}$), oxyphosphate, and their combinations.[29] Transition-metal phosphates, which include zirconium and titanium phosphates, are another class of photocatalysts.[30] Bismuth oxychloride-modified titanium phosphate nanoplates have also been used to degrade organic pollutants.[31] A chitosan-zirconium phosphate nanomaterial has been reported for chromium and dye remediation.[32] Molybdenum polyphosphates such as $(MoO_2)_2P_2O_7$[29] and $(MoO_2)_2P_2O_7$[33] have recently been studied for battery applications in the literature. Chiweshe et al. reported the molybdenum (meta)phosphate phase[34] using a fusion method. In other studies, the spectroscopic and magnetic properties of[35] $M(PO_3)_3$ (where M = Mo, Cr) were investigated. To date, there have been few reports of Mo(VI)-containing phosphates, and further investigation is still an intellectual and scientific curiosity. The phosphite $[(PO_3)^{3-}]$ present in molybdenum phosphate, like $[(PO_4)^{3-}]$,[36] may have a strong bonding nature with water and chemical redox property to the generated electrons and holes.

From the above discussion, it is clear that there is an urgent need for the rapid reduction of Cr(VI) from wastewater and conversion to Cr(III) to protect the environment from Cr(VI)-related toxicities. Despite extensive research on the development of a new photocatalytic system, competent, low-cost, metal-free, and environmentally benign compounds with superior photocatalytic activity must be revealed. Molybdenum phosphate can serve dual purposes such as photoreduction and less evoked toxicity. Molybdenum phosphates are cheap and nontoxic. The layered molybdenum (meta)phosphate material was synthesized in one pot with the one-step solvothermal process in ethylene glycol (EG) at 198 °C. It was also investigated as a photocatalyst for photoreduction of $Cr^{6+}$ to $Cr^{3+}$ and methylene blue degradation under natural sunlight radiance.

## 2. EXPERIMENTAL SECTION

**2.1. Materials.** Hexaammonium molybdate ($(NH_4)_6Mo_7O_{24}\cdot 4H_2O$, 98%), triphenylphosphine ($C_{18}H_{15}P$, 98%), ethylene glycol (EG, $C_2H_6O_2$, 98%), ethylene diammonium tetraacetic acid disodium salt (EDTA·2Na, 98%), and isopropanol ($C_3H_8O$) were purchased from S. D. Fine Chemicals Pvt. Ltd. Methanol ($CH_3OH$, 99%) and potassium dichromate ($K_2Cr_2O_7$, 99.5%) were purchased from SRL Pvt. Ltd. Methylene blue was from Loba Chemie Pvt. Ltd (95%), and formic acid (HCOOH) was from Merck India. Dimethyl sulfoxide (DMSO, 99.7%) and ascorbic acid were acquired from Sigma-Aldrich Ltd. All of the above chemicals were used as received.

**2.2. Synthesis of Layered Molybdenum (Meta)-phosphate [$MoO_2(PO_3)_2$].** Using hexaammonium molybdate $[(NH_4)_6Mo_7O_{24}\cdot 4H_2O]$ and triphenylphosphine ($C_{18}H_{15}P$) in EG under a nitrogen atmosphere, layered molybdenum (meta)phosphate was synthesized. In a 250 mL double-necked round-bottom flask, 10 mL of EG was refluxed in an inert atmosphere. Presonicated (5 min) 1.00 g of $(NH_4)_6Mo_7O_{24}\cdot 4H_2O$ in 10 mL of EG was added with a syringe to this preheated EG solution, and the solution turned lemon in color. Then, presonicated (5 min) 1.48 g of $C_{18}H_{15}P$ in 10 mL of EG was added dropwise to the round-bottom flask using a syringe. The color of the solution changed from lemon to pale yellow. The reaction mixture was refluxed for 2 h under an inert atmosphere with vigorous stirring. The brown-color product was cooled, centrifuged at 4800 ppm, washed with methanol, and dried naturally.

**2.3. Characterizations.** $MoO_2(PO_3)_2$ with a $2\theta$ value ranging from 8 to 90° was studied using an Xpert PRO PANalytical X-ray diffractometer (XRD) with Cu K radiation. The vibrational modes in $MoO_2(PO_3)_2$ were investigated using a Perkin Elmer Spectrum One FTIR spectrophotometer. A Perkin-Elmer LS 55 Luminescence spectrometer was used to measure the photoluminescence of $MoO_2(PO_3)_2$. Using a JEOL JSM-840 field emission scanning electron microscope (FE-SEM) with a 20 kV operating voltage, a textural study of elemental mapping and energy-dispersive X-ray analysis (EDAX) was performed. On a Philips-CM 200 with an operating voltage of 20−200 kV, high-resolution transmission electron microscopy (HRTEM) imaging was obtained. The composition was studied using X-ray photoelectron spectroscopy (XPS) with an AXIS Supra spectrometer (Kratos Analytical Ltd, U.K.) having an Al K$\alpha$ source ($h\nu$ = 1486.6 eV). Absorption spectroscopy, photoreduction, photodegradation, and trapping experiments were performed on a UV−vis spectrophotometer (UV-1800 PC Shimadzu) in the wavelength scan limit of 200−800 nm with a fast scan speed and a slit of 1 nm. The surface area of $MoO_2(PO_3)_2$ was recorded using the Brunauer−Emmett−Teller (BET) technique with the help of the SMART SORB 93, Smart Instruments Co. Pvt. Ltd, India. The electron spin resonance (ESR) analysis was performed on the ESR-JES-FA200 ESR spectrometer.

**2.4. Photoreduction Experiment of $Cr^{6+}$ to $Cr^{3+}$.** The photoreduction of $Cr^{6+}$ to $Cr^{3+}$ ions in solution was accomplished using the multilayered molybdenum (meta)-phosphate material that was synthesized. To begin, a 100 ppm hexavalent chromium solution in distilled water was made using potassium dichromate ($K_2Cr_2O_7$) powder. The photocatalytic reduction performance of $MoO_2(PO_3)_2$ was investigated, with formic acid acting as a hole scavenger.[37] To test the photocatalytic activity, 20 mg of the catalyst, 40 mL of 100 ppm $K_2Cr_2O_7$ solution, and 4 mL of formic acid were sonicated to disperse the catalyst and then left in the dark for 30 min to achieve adsorption−desorption equilibrium. For the photoreduction study in the UV−visible spectrophotometer, a 3 mL aliquot was taken at regular intervals. At the end of each cycle, a centrifuge was used to recover the catalyst from the solution.

**2.5. Photodegradation of Methylene Blue (MB).** The performance of the layered molybdenum (meta)phosphate material in the degradation of methylene blue has also been studied. In a 100 mL beaker, an aqueous solution of methylene


https://doi.org/10.1021/acsomega.2c02824
ACS Omega 2022, 7, 26632−26640

blue (40 mL, 10 ppm) and 20 mg of $MoO_2(PO_3)_2$ were used.[38] The mixture was sonicated to ensure uniform dispersion of the catalyst, and it was kept in the dark for 30 min to maintain adsorption−desorption equilibrium. A 3 mL aliquot was placed in a cuvette and tested for photodegradation using a UV−visible spectrophotometer. The catalyst was then recovered by washing it with distilled water and drying it in a hot air oven set to 60 °C.

## 3. RESULTS AND DISCUSSION

An X-ray diffraction pattern was used to examine the brown material. The XRD pattern of $MoO_2(PO_3)_2$ with an orthorhombic structure is shown in Figure 1 (ICDD: 01-074-1389).[34] The diffraction peaks can be assigned to the orthorhombic phase of $MoO_2(PO_3)_2$. Noteworthy Miller indices are observed at (100), (110), (210), (021), (220), (002), (112), etc. The presence of broad peaks in XRD implies the presence of smaller particles. Debye−Scherrer's formula was used to calculate the average particle size: $D = K\lambda/\beta \cos\theta$, where $D$ denotes the average crystallite size (nm), $K$ denotes the dimensionless shape factor with a value of 0.89, $\lambda$ denotes the X-ray diffraction wavelength, $\beta$ stands for the full width at half-maximum, and $\theta$ is the Bragg angle. The average particle size using the diffraction peak (100) was found to be 7.72 nm. Figure 2a depicts a low-resolution scanning electron image of the layered $MoO_2(PO_3)_2$ material. The layered material's morphology was found to be granularly stacked one on top of the other, similar to grains. Figure 2b depicts the layered material morphology after the first cycle of Cr(VI) photoreduction. In the IR spectrum, the peak due to ($P-O_{int}$) is observed at 995 $cm^{-1}$, which is in good agreement with the reported value (Figure S1).[35] Energy-dispersive spectrometry (EDS) elemental mapping was accomplished for the elements Mo, O, and P, which were distributed uniformly (Figure 2).

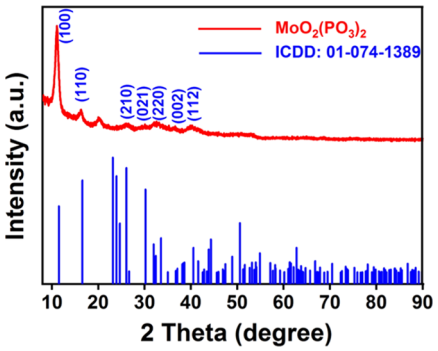


**Figure 1.** X-ray diffraction pattern of orthorhombic layered molybdenum (meta)phosphate [$MoO_2(PO_3)_2$].

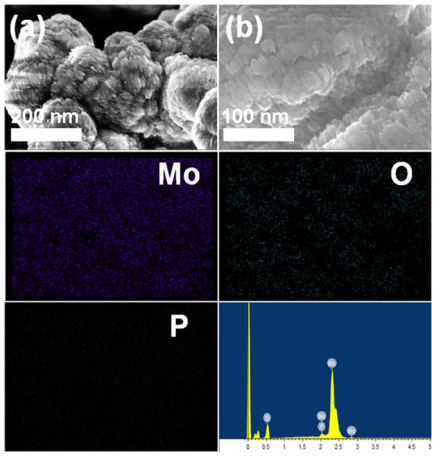


**Figure 2.** SEM images (a) and (b) of $MoO_2(PO_3)_2$, their elemental mapping images, and EDAX.

HRTEM was used to study the morphology of the $MoO_2(PO_3)_2$ nanoscale layered material. The layered structure of $MoO_2(PO_3)_2$ is depicted in Figure 3a. Figure 3b,c shows that the atomic lattices in the HRTEM image are crystalline. The value for $d$-spacing of the layered $MoO_2(PO_3)_2$ nanoscale material was found to be 0.25 nm, which is attributed to the (220) plane.

For the photoreduction of hexavalent chromium, a UV−visible spectrophotometer was used. The UV−visible spectrum of $MoO_2(PO_3)_2$ in isopropanol is shown in Figure 4a. Figure 4b represents the Tauc plot, which was obtained by plotting the $\alpha h\nu$ versus $h\nu$. In Tauc's relation, $\alpha$ was calculated with the help of an equation, i.e., $\alpha = 4\pi A/\lambda$ [where $A$ is the absorbance and $\lambda$ is the wavelength]. In this graph, the optical band gap was calculated by extrapolation of the curves on the X-axis (energy axis). The calculated optical band gap for the obtained layered $MoO_2(PO_3)_2$ was found to be 3.31 eV. The photoluminescence of $MoO_2(PO_3)_2$ was recorded in isopropanol and was found to be a broad spectrum at 470 nm with an excitation wavelength of 330 nm (Figure 5). The ESR activity of $MoO_2(PO_3)_2$ was investigated using the ESR spectrum to check for the presence of unpaired electrons (Figure S3).[35,39]

The elemental composition analysis of the Mo, P, and O elements of $MoO_2(PO_3)_2$ was performed using XPS. Figure 6a shows the molybdenum $3d_{3/2}$ and $3d_{5/2}$ at 231.44 and 228.27 eV.[40] For oxygen 1s, a peak was observed at 529.42 eV (Figure 6b), and for phosphorous 2p, a peak was observed at 136.79 eV (Figure 6c). Figure 6d shows the overall survey spectrum of $MoO_2(PO_3)_2$.

**3.1. Photoreduction of $Cr^{6+}$ to $Cr^{3+}$.** The primary goal of this research is to use a nontoxic, less expensive, and highly stable material as a photocatalyst. The surface area of $MoO_2(PO_3)_2$ nanocomposites was determined to be 15.34 $m^2/g$.[41] $MoO_2(PO_3)_2$ acts as a photocatalyst due to its adequate surface area and absorption in the UV−visible region in the presence of sunlight. We used a layered nanoscale $MoO_2(PO_3)_2$ material as a photocatalyst in this study, which demonstrated the complete reduction efficiency of chromium solution in the presence of natural sunlight. Figure 7A depicts the photoreduction of $Cr^{6+}$ to $Cr^{3+}$ using the layered $MoO_2(PO_3)_2$ nanoscale material with methanoic acid acting as a hole scavenger. The entire reduction of $Cr^{6+}$ ions from the solution was observed in 6 min. A rapid decrease in peak intensity around 349.50 nm indicates the conversion of toxic $Cr^{6+}$ to less toxic $Cr^{3+}$ by $MoO_2(PO_3)_2$.[18] The addition of sodium hydroxide solution resulted in the green-colored precipitate of $Cr(OH)_3$, indicating that the entire toxic form of chromium was converted to trivalent chromium. The X-ray diffraction pattern of used $MoO_2(PO_3)_2$ after the first cycle was studied to check the stability of the catalyst, and it was found to be similar to the bare $MoO_2(PO_3)_2$ (Figure S2). The kinetics of the reaction was investigated by plotting a graph of the ratio of the chromium concentration at time $t$ ($C_t$) to the original concentration ($C_0$) (i.e., $C_t/C_0$), as shown in Figure


https://doi.org/10.1021/acsomega.2c02824
ACS Omega 2022, 7, 26632−26640

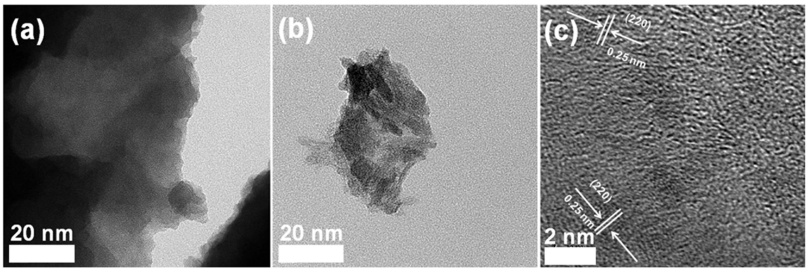


**Figure 3.** (a) TEM image, (b) HRTEM image, and (c) HRTEM image of layered molybdenum (meta)phosphate.

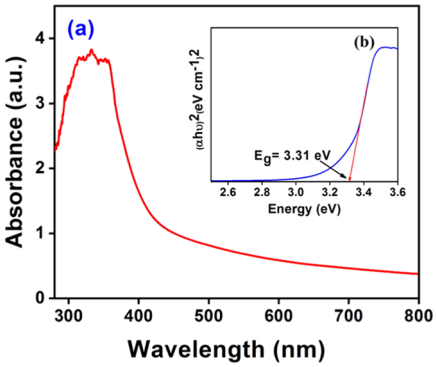


**Figure 4.** (a) UV−visible spectrum of molybdenum (meta)phosphate in isopropanol and (b) Tauc's plot.

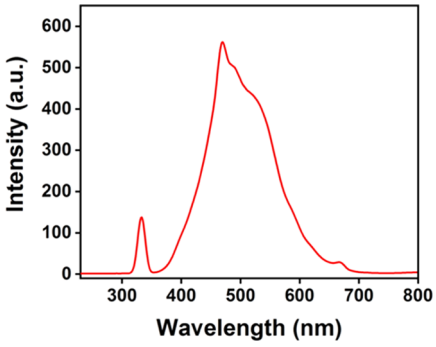


**Figure 5.** PL spectrum of $MoO_2(PO_3)_2$ in isopropanol (excitation wavelength = 330 nm).

7C. When the reactant is scarce, the improved Langmuir−Hinshelwood expression is transformed into the form $\ln(C_0/C_t) = kt$[38] (where $k$ = rate constant). The kinetics of a pseudo-first-order reaction was confirmed by plotting $\ln(C_0/C_t)$ versus time, as shown in the inset image in Figure 7C. The photocatalytic degradation efficiency of the $MoO_2(PO_3)_2$ catalyst was calculated as $(A_0 - A)/A_0 \times 100\%$ ($A_0$ and $A$ = absorbance of the chromium solution at time = 0 and 6 min, respectively).[21] The photocatalyst's stability and reusability are demonstrated in Figure 7E. We conducted chromium reduction in the UV−visible cabinet to compare the effects of sunlight and the UV−visible reactor. The reduction of $Cr^{6+}$ to $Cr^{3+}$ in the UV−visible cabinet is depicted in Figure S4. It took 9 min to complete, which is comparable to natural sunlight.

The chemical potential values for the donor and acceptor species are critical for understanding the ability and mechanism of $Cr^{6+}$ reduction. As a result, using eqs 1 and 2, the band-gap ($E_g$) value and Mulliken's electronegativity are used to calculate the valence ($E_{VB}$) and conduction band ($E_{CB}$) potentials.[37]

$$E_{CB} = \chi - E - 0.5E_g \quad (1)$$

$$E_{VB} = E_{CB} + E_g \quad (2)$$

$$\chi = ({}_A\chi^a \cdot {}_B\chi^b \ldots)^{1/(a+b+\ldots)} \quad (3)$$

$${}_A\chi = 0.5(EA_A + IE_A) \quad (4)$$

In the above equations, $E^e$ is the energy of free electrons on the hydrogen scale (4.5 eV), $E_g$ is the band gap (3.31 eV) of $MoO_2(PO_3)_2$, which was determined by the extrapolation line on the energy axis in the Tauc plot, and $\chi$ is the electronegativity of Mo, O, and P elements. The number of atoms is represented by a, b,... while A, B,.. are the ions present in the compound. From eqs 1 and 2, the calculated conduction band ($E_{CB}$) potential and the valence band ($E_{VB}$) potential are 0.7136 and 3.7536 V versus the standard hydrogen electrode (SHE). In a valence band, the reaction between generated holes and $OH^-$ gives rise to the active $^\bullet OH$ radical. Here, the reduction potential value for $Cr_2O_7^{2-}/Cr^{3+}$ (+1.33 eV) is detected in between the valence and conduction band potential of $MoO_2(PO_3)_2$. All of the above conditions are favorable for an enhancement of the reduction of the $Cr^{6+}$ to $Cr^{3+}$ event.[42] With the observed experimental conditions mentioned above and reported, the conversion of the $Cr^{6+}$ to $Cr^{3+}$ mechanism is as shown below.[43] The UV−visible light absorption property of $MoO_2(PO_3)_2$ leads to charge separation (eq 5), and methanoic acid aids in lowering the recombination of holes and electrons to form $CO_2$ and $H^+$ (eq 5).[43] The role of formic acid was examined in its absence for the photoreduction of $Cr^{6+}$ to $Cr^{3+}$ (Figure S5). In the absence of formic acid, the reduction of $Cr^{6+}$ to $Cr^{3+}$ did not occur within the time frame specified in Figure 7A. To inspect the role of formic acid, ethanol was used as a hole scavenger. Figure S6 shows that negligible degradation was observed, indicating that formic acid is a better hole scavenger than ethanol.[44]

$$h\nu + MoO_2(PO_3)_2 \rightarrow e^- + h^+ \quad (5)$$

$$2HCOO^- + 2h^+ \rightarrow 2CO_2 + 2H^+ \quad (6)$$

Electrons present in the conduction band could react with $Cr^{6+}$ to get $Cr^{3+}$ (eqs 7 and 8).[43] Figure 8 depicts a plausible schematic illustration of the $Cr^{6+}$ to $Cr^{3+}$ mechanism.

$$Cr^{6+} + 3e^- \rightarrow Cr^{3+} \quad (7)$$

$$Cr_2O_7^{2-} + 14H^+ + 6e^- \rightarrow 2Cr^{3+} + 7H_2O \quad (8)$$



https://doi.org/10.1021/acsomega.2c02824
ACS Omega 2022, 7, 26632−26640

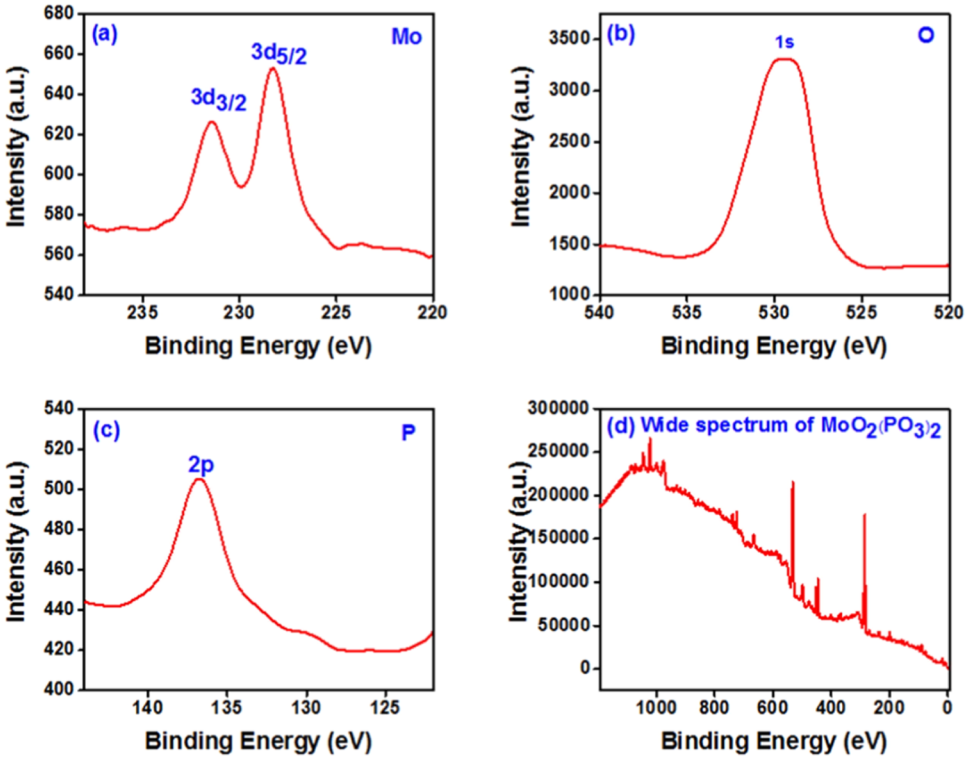


**Figure 6.** XPS spectra of (a) Mo $3d_{3/2}$ and $3d_{5/2}$, (b) O 1s, (c) P 2p, and (d) wide spectrum of $MoO_2(PO_3)_2$.

We attempted to use $MoO_2(PO_3)_2$ for representative MB dye degradation after achieving promising results in the chromium reduction experiment. Figure 7B depicts the UV–visible spectra of methylene blue dye photodegradation in the presence of natural sunlight. The absorption wavelength peak at 664 nm caused by MB was greatly reduced after 36 min, indicating methylene blue dye degradation.[37] The 95% photodegradation of 10 ppm of methylene blue was achieved in 36 min under sunlight.[21] The order of photodegradation of methylene blue was studied using a modified Langmuir–Hinshelwood equation (Figure 7D(a)). The graph of $\ln(C_0/C_t)$ versus solar light exposure time $t$ in Figure 7D(b) shows that the degradation follows pseudo-first-order kinetics. The catalyst's stability was tested over four consecutive cycles. Figure 7F shows a histogram of the percent degradation of MB over four cycles, i.e., 78, 77, 76, and 74%.

One of the reported plausible mechanisms is discussed further.[37] Under natural sunlight (eq 9) illumination, holes and electrons are generated during photocatalytic degradation processes.

$$h\nu + MoO_2(PO_3)_2 \rightarrow e^- + h^+ \quad (9)$$

The oxidation of the adsorbed water molecule on the catalyst produces $^\bullet$OH radicals at the valence band (eqs 10 to 12).

$$h^+ + OH^- \rightarrow {}^\bullet OH \quad (10)$$

$$h^+ + H_2O_{ads} \rightarrow {}^\bullet OH + H^+ \quad (11)$$

$$h^+ + OH_{ads} \rightarrow {}^\bullet OH \quad (12)$$

Photogenerated electrons react with adsorbed oxygen at the conduction band potential, resulting in superoxide anion radicals ($O_2^{\bullet-}$), and $H_2O_2$ is formed in the presence of adsorbed oxygen and hydrogen (eqs 13 and 14). Furthermore, $H_2O_2$ reacts with electrons in the conduction band, resulting in $^\bullet$OH radicals (eq 15). Figure 9 depicts a plausible schematic illustration of the MB mechanism.

$$e^- + O_{2ads} \rightarrow O_2^{\bullet-} \quad (13)$$

$$e^- + O_{2ads} + 2H^+ \rightarrow H_2O_2 \quad (14)$$

$$e^- + H_2O_{2ads} \rightarrow {}^\bullet OH + OH \quad (15)$$

According to the literature, nanomaterials such as metal oxides, nanocomposites, and metal phosphate are beneficial for the photodegradation of methylene blue. The representative examples were tabulated (Table 1) with the amount of catalyst used, the concentration of MB solution used, the reduction time, and the source of light.

To understand the mechanism, it is essential to comprehend the generated radicals and their roles in the degradation of MB. The reactive species trapping experiment was carried out to provide evidence for the existence of the main active species responsible for photocatalytic degradation of MB using $MoO_2(PO_3)_2$ (Figure 10). Typically, EDTA·2Na was used for $h^+$, ascorbic acid for superoxide anion radicals $O_2^{\bullet-}$, and dimethyl sulfoxide (DMSO) for $^\bullet$OH radicals as scavengers in the MB solution. The addition of EDTA·2Na (2 mL, 1 mM) as a hole scavenger reduced the photodegradation of methylene blue when exposed to sunlight.[36] Figure S7 depicts the photocatalytic degradation of MB by $MoO_2(PO_3)_2$ in the presence of EDTA·2Na as a hole scavenger. In the presence of ascorbic acid, MB photodegradation was significantly reduced. Photocatalytic degradation of MB by $MoO_2(PO_3)_2$ in the presence of DMSO as a $^\bullet$OH scavenger is shown in Figure S8. When DMSO is added, OH is the major active species contributing to the photocatalytic behavior of $MoO_2(PO_3)_2$. It


https://doi.org/10.1021/acsomega.2c02824
ACS Omega 2022, 7, 26632−26640

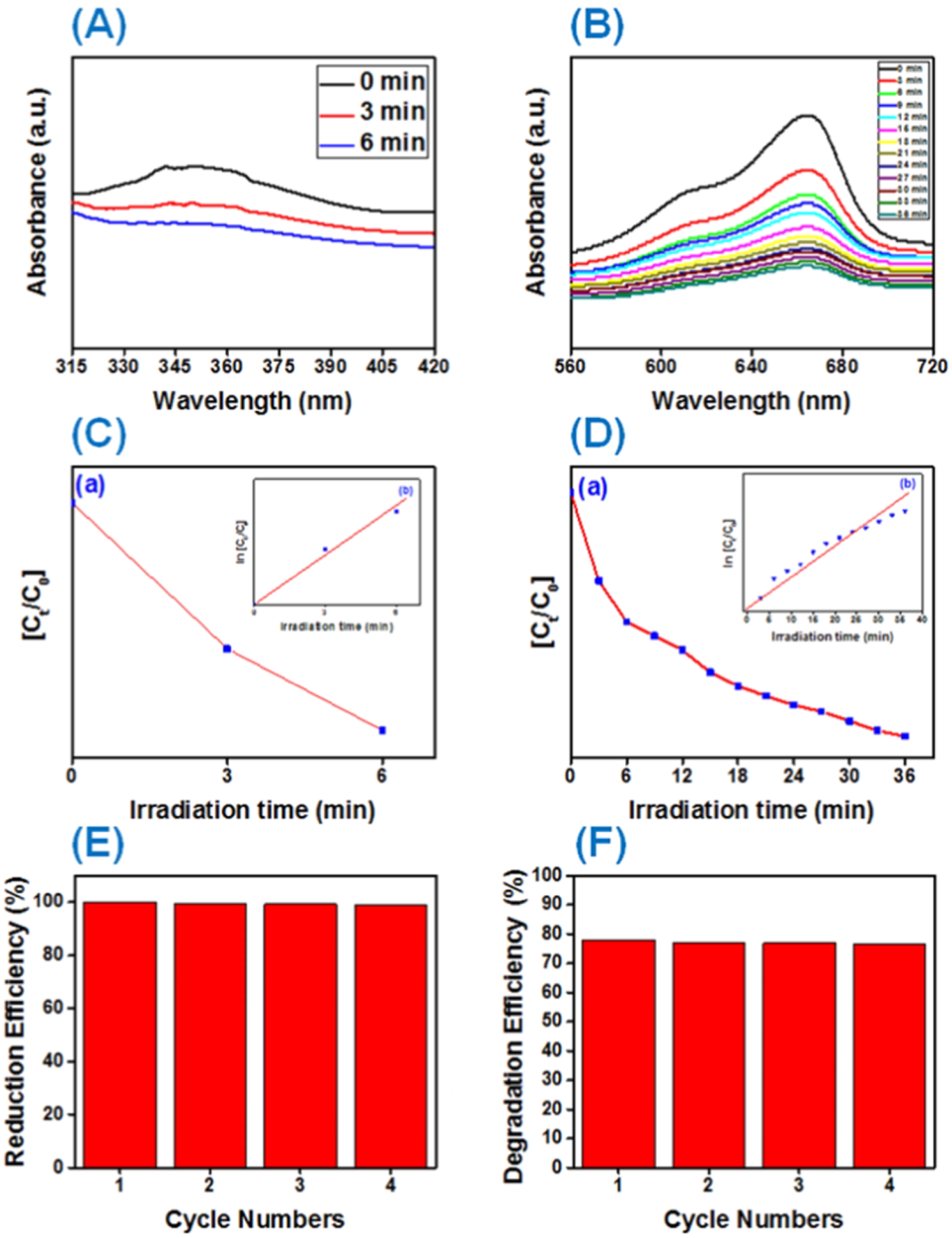


**Figure 7.** (A) Photoreduction of $Cr^{6+}$ to $Cr^{3+}$. (B) Photodegradation of methylene blue. (C) Plot of (a) $C_t/C_0$ and (b) ln $C_0/C_t$ (inset image) versus indication time for $Cr^{6+}$ to $Cr^{3+}$ reduction. (D) Plot of (a) $C_t/C_0$ and (b) ln $C_0/C_t$ (inset image) versus indication time for methylene blue degradation. (E) and (F) Reduction efficiency (%) for $Cr^{6+}$ to $Cr^{3+}$ reduction and for methylene blue degradation.

also implies that the active species in the oxidation of the adsorbed dye is the $^{\bullet}OH$ radical.[50] These results are in good agreement with $Bi(PO_4)$.[36] The $HO_2^{\bullet}$ radical may also act as an active radical in several reactions during the process. In addition to ascorbic acid (2 mL, 1 mM), the majority of $^{\bullet}OH$ radicals (Figure S9) may be converted into $HO_2^{\bullet}$ (eqs 16 and 17).[36]

$$^{\bullet}OH + C_6H_8O_6 \rightarrow H_2O + {}^{\bullet}C_6H_7O_6 \quad (16)$$

$$^{\bullet}C_6H_7O_6 + O_2 \rightarrow C_6H_6O_6 + HO_2^{\bullet} \quad (17)$$

$$O_2^{\bullet-} + C_6H_8O_6 + H^+ \rightarrow H_2O_2 + {}^{\bullet}C_6H_7O_6 \quad (18)$$

As a result, if $HO_2^{\bullet}$ aids in the oxidation of methylene blue, the degradation rate would be faster in the case of ascorbic acid, which is not observed during the process (addition of the $O_2^{\bullet-}$ scavenger), indicating that $O_2^{\bullet-}$ is important in the photodegradation process.[36] Furthermore, the reaction of $O_2^{\bullet-}$ with ascorbic acid in the presence of a proton generates $H_2O_2$ and ascorbate free radicals (eq 18). It would also aid in the production of $^{\bullet}OH$ radicals, as mentioned in eq 15.[51] No photocatalytic reduction of $Cr^{6+}$ to $Cr^{3+}$ by $MoO_2(PO_3)_2$ in the absence of sunlight was observed (Figure S10), indicating that $MoO_2(PO_3)_2$ can act as a stable, cheaper, and noble-metal-free photocatalyst.

## CONCLUSIONS

In this article, layered $MoO_2(PO_3)_2$ was synthesized in a single step using the solvothermal method. We used layered molybdenum (meta)phosphate as a photocatalyst material for the first time. In PL spectroscopy, a broad spectrum at 470 nm was observed. The obtained material is ESR-active, so



https://doi.org/10.1021/acsomega.2c02824
ACS Omega 2022, 7, 26632−26640

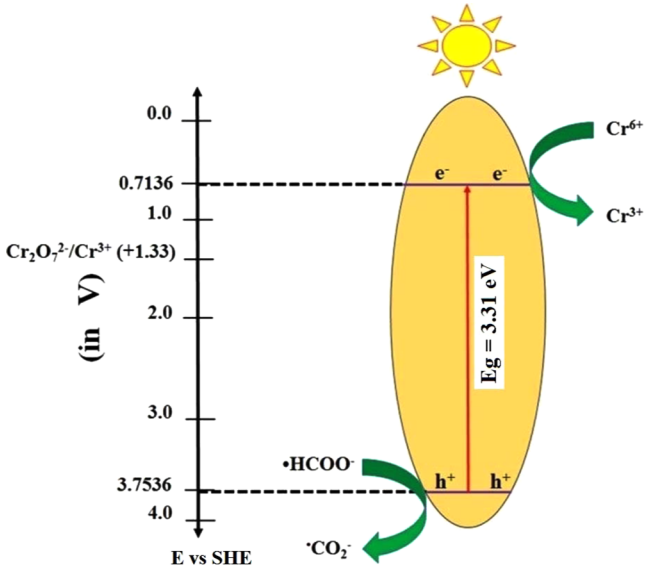


**Figure 8.** Plausible mechanism for photoreduction of $Cr^{6+}$ to $Cr^{3+}$ using $MoO_2(PO_3)_2$ under natural sunlight irradiation.

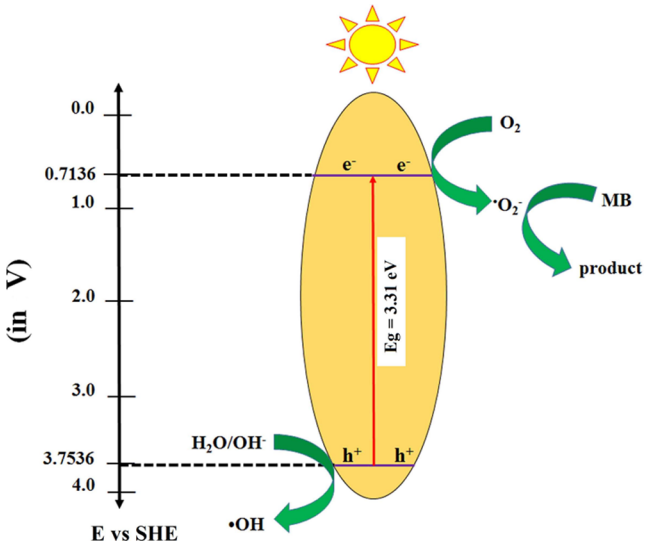


**Figure 9.** Plausible mechanism for the photodegradation of MB using $MoO_2(PO_3)_2$ under natural sunlight irradiation.

unpaired electrons may be present in it. Under natural sunlight, 20 mg of photocatalyst $Cr^{6+}$ was reduced to $Cr^{3+}$ in 6 min under optimal operating conditions such as 4 mL of formic acid. In the photoreduction of toxic chromium, formic acid was used as a hole scavenger. Furthermore, under natural sunlight, 78% photodegradation of methylene blue dye (40 mL, 10 ppm MB, and 20 mg of catalyst) was observed. By performing

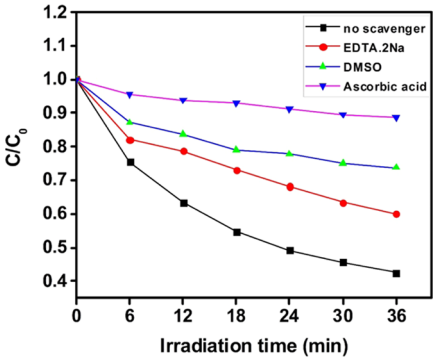


**Figure 10.** Plots of photogenerated carriers trapping in the system of photodegradation of methylene blue on $MoO_2(PO_3)_2$.

reactive species trapping experiments, the existence of $O_2^{\bullet-}$, $^{\bullet}OH$, and $h^+$ species, as well as the leading role of $O_2^{\bullet-}$ species, was confirmed. $O_2^{\bullet-}$ plays an important role in the fast degradation of methylene blue. The layered molybdenum (meta)phosphate photocatalyst is stable, inexpensive, and reusable.

## ■ ASSOCIATED CONTENT

### Supporting Information

The Supporting Information is available free of charge at https://pubs.acs.org/doi/10.1021/acsomega.2c02824.

IR spectrum of the $[MoO_2(PO_3)_2]$ catalyst (Figure S1); X-ray diffraction pattern of orthorhombic layered molybdenum (meta)phosphate $MoO_2(PO_3)_2$ after the first cycle (Figure S2); ESR spectrum of $MoO_2(PO_3)_2$ (Figure S3); plot of $C_0/C_t$ v/s irradiation time and plot of $\ln(C_0/C_t)$ v/s irradiation time for $Cr^{6+}$ to $Cr^{3+}$reduction in UV cabinet (Figure S4); photocatalytic study of the $Cr^{6+}$ to $Cr^{3+}$ reduction by $MoO_2(PO_3)_2$ in the presence of natural sunlight without formic acid as a hole scavenger (Figure S5); photocatalytic reduction of $Cr^{6+}$ to $Cr^{3+}$ by $MoO_2(PO_3)_2$ in the presence of EtOH as a hole scavenger (Figure S6); photocatalytic degradation of MB by $MoO_2(PO_3)_2$ in the presence of EDTA·2Na as a hole scavenger (Figure S7); photocatalytic degradation of MB by $MoO_2(PO_3)_2$ in the presence of DMSO as a $^{\bullet}OH$ scavenger (Figure S8); photocatalytic degradation of MB by $MoO_2(PO_3)_2$ in the presence of ascorbic acid as a $^{\bullet}O_2^-$ scavenger (Figure S9); and no photocatalytic reduction of $Cr^{6+}$ to $Cr^{3+}$ by $MoO_2(PO_3)_2$ in the absence of sunlight (Figure S10) (PDF)

**Table 1. Comparison of Catalytic Degradation of MB with Different Catalysts**

| catalyst used | amount of catalyst | MB concentration | photodegradation time (min) | source of light | refs |
|---|---|---|---|---|---|
| CA/TPNC | 100 mg | $2 \times 10^{-5}$ M | 150 | sunlight | 45 |
| $CeO_2$/g-$C_3N_4$ | 0.05 g | 10 mg $L^{-1}$ | 180 | UV-light | 46 |
| $Mn_3O_4$/ZnO/$Eu_2O_3$ | 15 mg | 5 ppm | 150 | sunlight | 47 |
| $Ag_3PO_4$/NC | 0.018 g | 37.5 ppm | 105 | sunlight | 48 |
| CTHS | 5 mg | 10 mM | 30 | sunlight | 49 |
| $MoO_2(PO_3)_2$ | 20 mg | 10 ppm | 36 | sunlight | present work |



https://doi.org/10.1021/acsomega.2c02824
ACS Omega 2022, 7, 26632−26640

## AUTHOR INFORMATION


### Corresponding Author

**Anil M. Palve** − *Department of Chemistry, Mahatma Phule Arts, Science, and Commerce College, Navi-Mumbai, Maharashtra 410206, India;* orcid.org/0000-0003-3190-4857; Email: palve_anil@yahoo.com

### Author

**Omkar V. Vani** − *Department of Chemistry, Mahatma Phule Arts, Science, and Commerce College, Navi-Mumbai, Maharashtra 410206, India*

Complete contact information is available at: https://pubs.acs.org/10.1021/acsomega.2c02824


### Notes

The authors declare no competing financial interest.

The authors declare that they have no known competing financial interests or personal relationships that could have appeared to influence the work reported in this paper.

## ACKNOWLEDGMENTS

The authors thank TIFR Mumbai for providing the XRD for the samples. Thanks are also due to SAIF, IIT-Bombay, Mumbai, for HRTEM images and ESR and SEM analyses and to IIT-Delhi for XPS analysis. The authors thank Dr. Sandesh Jaybhaye, B.K. Birla College of Arts, Science, and Commerce, Kalyan, India, for carrying out surface area measurements for $MoO_2(PO_3)_2$.

## REFERENCES


(1) Yadav, M.; Xu, Q. Catalytic Chromium Reduction Using Formic Acid and Metal Nanoparticles Immobilized in a Metal−Organic Framework. *Chem. Commun.* **2013**, *49*, 3327.

(2) Acharya, R.; Naik, B.; Parida, K. Cr(VI) Remediation from Aqueous Environment through Modified-TiO 2 -Mediated Photocatalytic Reduction. *Beilstein J. Nanotechnol.* **2018**, *9*, 1448−1470.

(3) Shao, D.; Wang, X.; Fan, Q. Photocatalytic Reduction of Cr(VI) to Cr(III) in Solution Containing ZnO or ZSM-5 Zeolite Using Oxalate as Model Organic Compound in Environment. *Microporous Mesoporous Mater.* **2009**, *117*, 243−248.

(4) Badhe, R. A.; Ansari, A.; Garje, S. S. One-Pot Synthesis of Pd-Based Ternary Pd@CdS@TiO 2 Nanoclusters via a Solvothermal Route and Their Catalytic Reduction Efficiency toward Toxic Hexavalent Chromium. *ACS Omega* **2018**, *3*, 18663−18672.

(5) Mphela, R. K.; Msimanga, W.; Pete, K. Y.; Chiririwa, H.; Ochieng, A. Photocatalytic Degradation of Salicylic Acid and Reduction of Cr(VI) Using TiO2. *Int. J. Res. Chem. Metall. Civ. Eng.* **2016**, *3*, 3−7.

(6) Gong, K.; Wang, W.; Yan, J.; Han, Z. Highly Reduced Molybdophosphate as a Noble-Metal-Free Catalyst for the Reduction of Chromium Using Formic Acid as a Reducing Agent. *J. Mater. Chem. A* **2015**, *3*, 6019−6027.

(7) Almeida, C. A. P.; Debacher, N. A.; Downs, A. J.; Cottet, L.; Mello, C. A. D. Removal of Methylene Blue from Colored Effluents by Adsorption on Montmorillonite Clay. *J. Colloid Interface Sci.* **2009**, *332*, 46−53.

(8) Yogi, C.; Kojima, K.; Wada, N.; Tokumoto, H.; Takai, T.; Mizoguchi, T.; Tamiaki, H. Photocatalytic Degradation of Methylene Blue by TiO2 Film and Au Particles-TiO2 Composite Film. *Thin Solid Films* **2008**, *516*, 5881−5884.

(9) Ahmed, M. A.; El-Katori, E. E.; Gharni, Z. H. Photocatalytic Degradation of Methylene Blue Dye Using Fe2O 3/TiO2 Nanoparticles Prepared by Sol-Gel Method. *J. Alloys Compd.* **2013**, *553*, 19−29.

(10) Hassani, A.; Krishnan, S.; Scaria, J.; Eghbali, P.; Nidheesh, P. V. Z-Scheme Photocatalysts for Visible-Light-Driven Pollutants Degradation: A Review on Recent Advancements. *Curr. Opin. Solid State Mater. Sci.* **2021**, *25*, No. 100941.

(11) Ghanbari, F.; Hassani, A.; Wacławek, S.; Wang, Z.; Matyszczak, G.; Lin, K.-Y. A.; Dolatabadi, M. Insights into Paracetamol Degradation in Aqueous Solutions by Ultrasound-Assisted Heterogeneous Electro-Fenton Process: Key Operating Parameters, Mineralization and Toxicity Assessment. *Sep. Purif. Technol.* **2021**, *266*, No. 118533.

(12) Ntakadzeni, M.; Anku, W. W.; Kumar, N.; Govender, P. P.; Reddy, L. PEGylated MoS2 Nanosheets: A Dual Functional Photocatalyst for Photodegradation of Organic Dyes and Photoreduction of Chromium from Aqueous Solution. *Bull. Chem. React. Eng. Catal.* **2019**, *14*, 142−152.

(13) Omole, M. A.; K'Owino, I. O.; Sadik, O. A. Palladium Nanoparticles for Catalytic Reduction of Cr(VI) Using Formic Acid. *Appl. Catal., B* **2007**, *76*, 158−167.

(14) Deng, F.; Lu, X.; Luo, Y.; Wang, J.; Che, W.; Yang, R.; Luo, X.; Luo, S.; Dionysiou, D. D. Novel Visible-Light-Driven Direct Z-Scheme CdS/CuInS2 Nanoplates for Excellent Photocatalytic Degradation Performance and Highly-Efficient Cr(VI) Reduction. *Chem. Eng. J.* **2019**, *361*, 1451−1461.

(15) Khalil, L. B.; Mourad, W. E.; Rophael, M. W. Photocatalytic Reduction of Environmental Pollutant Cr(VI) over Some Semiconductors under UV/Visible Light Illumination. *Appl. Catal., B* **1998**, *17*, 267−273.

(16) Qiu, J.; Zhang, X. F.; Zhang, X.; Feng, Y.; Li, Y.; Yang, L.; Lu, H.; Yao, J. Constructing Cd0.5Zn0.5S@ZIF-8 Nanocomposites through Self-Assembly Strategy to Enhance Cr(VI) Photocatalytic Reduction. *J. Hazardous Mater.* **2018**, *349*, 234−241.

(17) Ren, Z.; Liu, X.; Zhuge, Z.; Gong, Y.; Sun, C. Q. MoSe2/ZnO/ZnSe Hybrids for Efficient Cr(VI) Reduction under Visible Light Irradiation. *Chin. J. Catal.* **2020**, *41*, 180−187.

(18) Veerakumar, P.; Thanasekaran, P.; Lin, K. C.; Liu, S. Bin. Biomass Derived Sheet-like Carbon/Palladium Nanocomposite: An Excellent Opportunity for Reduction of Toxic Hexavalent Chromium. *ACS Sustainable Chem. Eng.* **2017**, *5*, 5302−5312.

(19) Ramya, V.; Murugan, D.; Lajapathirai, C.; Sivasamy, A. Activated Carbon (Prepared from Secondary Sludge Biomass) Supported Semiconductor Zinc Oxide Nanocomposite Photocatalyst for Reduction of Cr(VI) under Visible Light Irradiation. *J. Environ. Chem. Eng.* **2018**, *6*, 7327−7337.

(20) Houas, A. Photocatalytic Degradation Pathway of Methylene Blue in Water. *Appl. Catal., B* **2001**, *31*, 145−157.

(21) Isai, K. A.; Shrivastava, V. S. Photocatalytic Degradation of Methylene Blue Using ZnO and 2%Fe−ZnO Semiconductor Nanomaterials Synthesized by Sol−Gel Method: A Comparative Study. *SN Appl. Sci.* **2019**, *1*, No. 1247.

(22) Lai, Y.; Sun, L.; Chen, Y.; Zhuang, H.; Lin, C.; Chin, J. W. Effects of the Structure of TiO[Sub 2] Nanotube Array on Ti Substrate on Its Photocatalytic Activity. *J. Electrochem. Soc.* **2006**, *153*, D123.

(23) Saravanan, R.; Shankar, H.; Prakash, T.; Narayanan, V.; Stephen, A. ZnO/CdO Composite Nanorods for Photocatalytic Degradation of Methylene Blue under Visible Light. *Mater. Chem. Phys.* **2011**, *125*, 277−280.

(24) Li, H.; Liu, Y.; Cui, Y.; Zhang, W.; Fu, C.; Wang, X. Facile Synthesis and Enhanced Visible-Light Photoactivity of DyVO4/g-C3N4I Composite Semiconductors. *Appl. Catal., B* **2016**, *183*, 426−432.

(25) Matos, J.; Ocares-Riquelme, J.; Poon, P. S.; Montaña, R.; García, X.; Campos, K.; Hernández-Garrido, J. C.; Titirici, M. M. C-Doped Anatase TiO 2: Adsorption Kinetics and Photocatalytic Degradation of Methylene Blue and Phenol, and Correlations with DFT Estimations. *J. Colloid Interface Sci.* **2019**, *547*, 14−29.

(26) Schneider, J.; Matsuoka, M.; Takeuchi, M.; Zhang, J.; Horiuchi, Y.; Anpo, M.; Bahnemann, D. W. Understanding TiO 2 Photocatalysis: Mechanisms and Materials. *Chem. Rev.* **2014**, *114*, 9919−9986.

(27) Dong, H.; Zeng, G.; Tang, L.; Fan, C.; Zhang, C.; He, X.; He, Y. An Overview on Limitations of TiO2-Based Particles for Photocatalytic Degradation of Organic Pollutants and the Corresponding Countermeasures. *Water Res.* **2015**, *79*, 128−146.
(28) Lee, S. Y.; Kang, D.; Jeong, S.; Do, H. T.; Kim, J. H. Photocatalytic Degradation of Rhodamine B Dye by TiO 2 and Gold Nanoparticles Supported on a Floating Porous Polydimethylsiloxane Sponge under Ultraviolet and Visible Light Irradiation. *ACS Omega* **2020**, *5*, 4233−4241.
(29) Wen, B.; Chernova, N. A.; Zhang, R.; Wang, Q.; Omenya, F.; Fang, J.; Whittingham, M. S. Layered Molybdenum (Oxy)-Pyrophosphate as Cathode for Lithium-Ion Batteries. *Chem. Mater.* **2013**, *25*, 3513−3521.
(30) Lin, R.; Ding, Y. A Review on the Synthesis and Applications of Mesostructured Transition Metal Phosphates. *Materials* **2013**, *6*, 217−243.
(31) Ao, Y.; Bao, J.; Wang, P.; Wang, C.; Hou, J. Bismuth Oxychloride Modified Titanium Phosphate Nanoplates: A New p-n Type Heterostructured Photocatalyst with High Activity for the Degradation of Different Kinds of Organic Pollutants. *J. Colloid Interface Sci.* **2016**, *476*, 71−78.
(32) Bhatt, R.; Ageetha, V.; Rathod, S. B.; Padmaja, P. Self-Assembled Chitosan-Zirconium Phosphate Nanostructures for Adsorption of Chromium and Degradation of Dyes. *Carbohydr. Polym.* **2019**, *208*, 441−450.
(33) Deng, W.; Feng, X.; Xiao, Y.; Li, C. Layered Molybdenum (Oxy) Pyrophosphate (MoO 2) 2 P 2 O 7 as a Cathode Material for Sodium-Ion Batteries. *ChemElectroChem* **2018**, *5*, 1032−1036.
(34) Chiweshe, T. T. Characterization of Molybdenum and Tungsten Phosphates Compounds Prepared Using Ammonium Phosphate Salt as Flux. *Bull. Chem. Soc. Ethiop.* **2019**, *33*, 103−112.
(35) Rojo, J. M.; Mesa, J. L.; Lezama, L.; Rojo, T. Spectroscopic and Magnetic Properties of Three M(PO3)3 (M = Cr and Mo) Metaphosphates. *J. Mater. Chem.* **1997**, *7*, 2243−2248.
(36) Pan, C.; Zhu, Y. New Type of BiPO4 Oxy-Acid Salt Photocatalyst with High Photocatalytic Activity on Degradation of Dye. *Environ. Sci. Technol.* **2010**, *44*, 5570−5574.
(37) Anandkumar, M.; Lathe, A.; Palve, A. M.; Deshpande, A. S. Single-Phase Gd0.2La0.2Ce0.2Hf0.2Zr0.2O2 and Gd0.2La0.2Y0.2Hf0.2Zr0.2O2 Nanoparticles as Efficient Photocatalysts for the Reduction of Cr(VI) and Degradation of Methylene Blue Dye. *J. Alloys Compd.* **2021**, *850*, No. 156716.
(38) Palve, A. M.; Kokil, D. N. One-Pot Synthesis of ZnS-RGO Nanocomposites Using Single-Source Molecular Precursor for Photodegradation of Methylene Blue and Reduction towards Toxic Cr(VI) under Solar Light. *Mater. Res. Express* **2019**, *6*, No. 105536.
(39) Li, S.; Wang, C.; Cai, M.; Yang, F.; Liu, Y.; Chen, J.; Zhang, P.; Li, X.; Chen, X. Facile Fabrication of TaON/Bi2MoO6 Core−Shell S-Scheme Heterojunction Nanofibers for Boosting Visible-Light Catalytic Levofloxacin Degradation and Cr(VI) Reduction. *Chem. Eng. J.* **2022**, *428*, No. 131158.
(40) Baltrusaitis, J.; Mendoza-Sanchez, B.; Fernandez, V.; Veenstra, R.; Dukstiene, N.; Roberts, A.; Fairley, N. Generalized Molybdenum Oxide Surface Chemical State XPS Determination via Informed Amorphous Sample Model. *Appl. Surf. Sci.* **2015**, *326*, 151−161.
(41) Chai, B.; Yan, J.; Fan, G.; Song, G.; Wang, C. In Situ Fabrication of CdMoO4/g-C3N4 Composites with Improved Charge Separation and Photocatalytic Activity under Visible Light Irradiation. *Chin. J. Catal.* **2020**, *41*, 170−179.
(42) Kumar, S.; Sharma, R.; Sharma, V.; Harith, G.; Sivakumar, V.; Krishnan, V. Role of RGO Support and Irradiation Source on the Photocatalytic Activity of CdS-ZnO Semiconductor Nanostructures. *Beilstein J. Nanotechnol.* **2016**, *7*, 1684−1697.
(43) Xu, Q.; Li, R.; Wang, C.; Yuan, D. Visible-Light Photocatalytic Reduction of Cr(VI) Using Nano-Sized Delafossite (CuFeO2) Synthesized by Hydrothermal Method. *J. Alloys Compd.* **2017**, *723*, 441−447.
(44) Kaur, H.; Sinha, S.; Krishnan, V.; Koner, R. R. Photocatalytic Reduction and Recognition of Cr(VI): New Zn(II)-Based Metal−Organic Framework as Catalytic Surface. *Ind. Eng. Chem. Res.* **2020**, *59*, 8538−8550.
(45) Gupta, V. K.; Saleh, T. A.; Pathania, D.; Rathore, B. S.; Sharma, G. A Cellulose Acetate Based Nanocomposite for Photocatalytic Degradation of Methylene Blue Dye under Solar Light. *Ionics* **2015**, *21*, 1787−1793.
(46) Wei, X.; Wang, X.; Pu, Y.; Liu, A.; Chen, C.; Zou, W.; Zheng, Y.; Huang, J.; Zhang, Y.; Yang, Y.; Naushad, M.; Gao, B.; Dong, L. Facile Ball-Milling Synthesis of CeO2/g-C3N4 Z-Scheme Heterojunction for Synergistic Adsorption and Photodegradation of Methylene Blue: Characteristics, Kinetics, Models, and Mechanisms. *Chem. Eng. J.* **2021**, *420*, No. 127719.
(47) Singh, J.; Juneja, S.; Soni, R. K.; Bhattacharya, J. Sunlight Mediated Enhanced Photocatalytic Activity of TiO2 Nanoparticles Functionalized CuO-Cu2O Nanorods for Removal of Methylene Blue and Oxytetracycline Hydrochloride. *J. Colloid Interface Sci.* **2021**, *590*, 60−71.
(48) Lebogang, L.; Bosigo, R.; Lefatshe, K.; Muiva, C. Ag3PO4/Nanocellulose Composite for Effective Sunlight Driven Photodegradation of Organic Dyes in Wastewater. *Mater. Chem. Phys.* **2019**, *236*, No. 121756.
(49) Singh, J.; Juneja, S.; Soni, R. K.; Bhattacharya, J. Sunlight Mediated Enhanced Photocatalytic Activity of TiO2 Nanoparticles Functionalized CuO-Cu2O Nanorods for Removal of Methylene Blue and Oxytetracycline Hydrochloride. *J. Colloid Interface Sci.* **2021**, *590*, 60−71.
(50) Faisal, M.; Harraz, F. A.; Ismail, A. A.; El-Toni, A. M.; Al-Sayari, S. A.; Al-Hajry, A.; Al-Assiri, M. S. Novel Mesoporous NiO/TiO2 Nanocomposites with Enhanced Photocatalytic Activity under Visible Light Illumination. *Ceram. Int.* **2018**, *44*, 7047−7056.
(51) Nandi, A.; Chatterjee, I. B. Scavenging of Superoxide Radical by Ascorbic Acid. *J. Biosci.* **1987**, *11*, 435−441.


https://doi.org/10.1021/acsomega.2c02824
*ACS Omega* 2022, 7, 26632−26640